Mathematical Modeling and Experimental Characterization of Polymer Dissolution

Nikolaos A. Peppas* and J. C. Wu†

School of Chemical Engineering, Purdue University, West Lafayette, Indiana 47907-1283

Ernst D. von Meerwall

Department of Physics and Maurice Morton Institute of Polymer Science, The University of Akron, Akron, Ohio 44325

Received March 28, 1994®

ABSTRACT: A new polymer dissolution model was developed by incorporating the polymer chain disentanglement mechanism into the relevant transport equations. The disentanglement time was used as a dissolution characteristic time controlling the moving position of the solvent–polymer boundary. A dimensionless dissolution number was defined as the ratio of the characteristic polymer disentanglement time to the characteristic solvent diffusion time. The dissolution number was shown to be proportional to the square of the gel layer thickness. Scaling law expressions for the dependence of the gel layer thickness and the polymer dissolution rate on polymer molecular weight were also derived. Solution of the model for one-dimensional dissolution showed three distinct dissolution stages and confirmed the proposed scaling law relations for the gel layer thickness and the dissolution rate. Experimental studies of dissolution of polystyrene and poly(methyl methacrylate) in methyl ethyl ketone were used to verify the model, and two types of polymer dissolution behavior were observed. For dissolution of polystyrene in MEK, the solvent diffusion behavior was Fickian and a constant gel layer thickness was observed during the stationary dissolution stage. The effect of polymer molecular weight on the gel layer thickness was investigated for nine monodisperse samples, with $\bar{M}_n$ ranging from 28 000 to 2 830 000. The experimental results showed that the dependence of the gel layer thickness on molecular weight is more prominent in the high molecular weight region. The polystyrene data verified the new dissolution model. The dissolution of PMMA in MEK was controlled by crack propagation as no significant gel layer was observed.

Introduction

Polymer dissolution in a solvent is an important phenomenon in a variety of applications. In microlithography, the irradiated regions of a thin polymer film are dissolved by an appropriate solvent to form desired patterns.[1] In controlled-release applications of polymers, a solute is dispersed or molecularly dissolved in a polymer phase. The release process can be controlled either by solvent diffusion or by polymer dissolution.[2,3] For many copolymers with either anionic or cationic groups, polymer dissolution can be controlled by a pH adjustment.[4] In addition, acrylic copolymers[5] can be used as selective soluble plastic packaging materials.

The dissolution process of a glassy polymer is the combined result of two phenomena: solvent penetration and polymer dissolution. The early work of Ueberreiter and co-workers[6-8] described the various types of dissolution and the surface layer structure. Important parameters affecting the dissolution process included the solvent diffusion coefficient, polymer molecular weight, solvent thermodynamic compatibility, agitation, and temperature. Experimental characterization of polymer dissolution has been presented by numerous researchers,[9-23] and various mechanisms and mathematical models have been proposed.

Tu and Ouano[24] proposed a mathematical model for polymer dissolution consisting of a solvent diffusion equation in the polymer, a polymer diffusion equation in a liquid layer adjacent to the polymer, and an equation for the moving position of the solvent–polymer interface. They showed that the moving velocity of the interface is equal to the difference between the solvent swelling rate, calculated by the solvent diffusion flux at the interface, and the polymer dissolution rate, expressed by the polymer diffusion rate at the interface. The key parameter of this model was the polymer disassociation rate, which was defined as the rate at which polymer molecules detached from the gel–solvent interface. Thus, a dissolution process can be either disassociation-rate-controlled, if the polymer diffusion rate in the liquid layer is faster than the disassociation rate, or diffusion-controlled, if the diffusion rate is slower than the disassociation rate.

Lee and Peppas[25] extended Tu and Ouano's model by introducing the idea that polymer dissolution was also controlled by an external mass transfer resistance. A film model was used to express the polymer dissolution rate. An approximate solution was obtained which indicated that the thickness of the gel layer formed during a dissolution process was proportional to the square root of time.

Papanu et al.[26] proposed a polymer dissolution rate model based on reptation theory. The polymer dissolution rate was expressed as a ratio of the radius of gyration of the polymer to the reptation time. The dependence of the radius of gyration and the reptation time on molecular weight and polymer concentration were derived by use of reptation scaling law. This model assumed that the dissolution rate is only related to the polymer concentration at the solvent–polymer interface, but independent of the solvent concentration inside the polymer. Similar to Tu and Ouano's model, this model cannot predict the swelling time generally required for a polymer dissolution process.

Brochard and de Gennes[27] proposed a relaxation-controlled polymer dissolution kinetics model with a dissolution flux proportional to the difference between the polymer stress gradient and the solvent osmotic

* Author to whom all correspondence should be addressed.
† Present address: Quantum Chemical Corp., USI Division, Process Research Center, Morris, IL 60450.
® Abstract published in *Advance ACS Abstracts*, September 1, 1994.

0024-9297/94/2227-5626$04.50/0

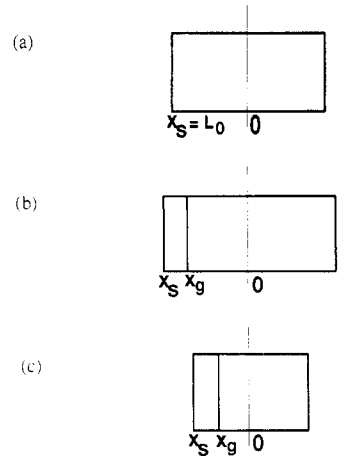

Figure 1. Schematic representation of a one-dimensional solvent diffusion and polymer dissolution process: (a) initial slab thickness, $2L_0$; (b) initial swelling step showing the increasing position of the solvent–polymer interface, x_s, and the decreasing position of the gel–glassy interface, x_g; (c) after true dissolution starts, movement of both interfaces toward the center of the slab.

pressure gradient. After a swelling gel layer was formed, the sequential dissolution of the polymer from the swollen state was governed by the relaxation rate of the stress. This rate should be of the order of the reptation time.

Herman and Edwards[28] further extended Brochard and de Gennes' model by considering in detail the stress accompanying the swelling of the polymer within the reptation model. Therefore, solvent swelling induced a nonrandom distribution of polymer chain orientation. This contribution to the free energies and chemical potentials of polymer and solvent was evaluated in a closed form from the reptation theory. When sufficiently large compared with the ordinary mixing terms, the system underwent a "phase separation" into a gel-like concentrated and a dilute solution phase.

In the present work, a polymer dissolution model is proposed which is based on the polymer chain disentanglement mechanism. In this model, the concept of a "dissolution clock" that controls the dissolution process is introduced. In addition, a dissolution number is introduced, which is a ratio of characteristic polymer disentanglement time to characteristic solvent diffusion time. The magnitude of this dimensionless number determines the gel layer thickness.

Model Development

Solvent Diffusion Model. We consider a one-dimensional solvent diffusion and polymer dissolution process as shown in Figure 1. In the initial stages of the process a glassy polymer slab of thickness $2L_0$ starts swelling because of the solvent transport in the slab and the simultaneous transition from the glassy to the rubbery state at a characteristic solvent volume fraction, $v_{1,g}$. Thus, two distinct fronts are observed: a solvent–polymer front (the solvent–gel front) at position x_s and a gel–glassy front at position x_g. Front x_g moves inward whereas front x_s moves outward. After an induction time, the true dissolution process occurs. Front x_g continues moving toward the center of the slab whereas front x_s now moves inward as well.

Solvent diffusion during a dissolution process obeys Fick's law.

$$\frac{\partial v_1}{\partial t} = \frac{\partial}{\partial x}\left[D_{12}\frac{\partial v_1}{\partial x}\right] \tag{1}$$

The initial and boundary conditions are

$$v_1(t=0,x) = 0 \tag{2}$$

$$v_1(t,x=x_s) = v_{1,\mathrm{eff}} \tag{3}$$

$$\partial v_1(t,x=0)/\partial x = 0 \tag{4}$$

where v_1 is the solvent volume fraction, $v_{1,\mathrm{eff}}$ is the effective solvent surface volume fraction at the solvent–polymer interface, x_s is the interface position, and D_{12} is the mutual diffusion coefficient, which is a function of the solvent volume fraction according to

$$D_{12} = D_0 \exp(a_d v_1) \tag{5}$$

Solvent diffusion in glassy polymers may deviate from the predictions of Fick's law, leading to anomalous or non-Fickian diffusional behavior.[29,30] Thomas and Windle[31] developed a solvent diffusion model which accounts for the effect of polymer viscoelastic properties on the solvent diffusional behavior. Durning[32] modified this model by using the Maxwell model as a mechanical analog of polymer viscoelastic properties. Wu and Peppas[33] recently extended Durning's model to integrate sorption, where the difference between the initial and final solvent concentration is large and the diffusion resistance due to polymer swelling needs be considered.

Our model[33] can be readily applied to solvent diffusion during a dissolution process. The model equation for one-dimensional solvent diffusion is

$$\frac{\partial v_1}{\partial t} = \frac{\partial}{\partial x}\left[D_{12}\frac{\partial v_1}{\partial x}\right] + \frac{\partial}{\partial x}\left[\frac{D_{12}\bar{V}_1 v_1}{RT(1-v_1)(1-2\chi v_1)}\frac{\partial \sigma_{xx}}{\partial x}\right] \tag{6}$$

with

$$\frac{\partial \sigma_{xx}}{\partial t} = -\frac{\sigma_{xx}}{(\eta/E)} + \frac{E}{(1-v_1)^2}\frac{\partial v_1}{\partial t} \tag{7}$$

Here, σ_{xx} is the normal stress in the x direction, $\bar{V}_1$ is the solvent molar volume, χ is the Flory interaction parameter, E is Young's modulus of the spring in the Maxwell model, and η is the viscosity of the dashpot in the Maxwell model, which is a function of solvent concentration,

$$\eta = \eta_0 \exp(-a_\eta v_1) \tag{8}$$

The initial conditions of eqs 6 and 7 are

$$v_1(t=0,x) = 0 \tag{9}$$

$$\sigma_{xx}(t=0,x) = 0 \tag{10}$$

The boundary conditions of eqs 6 and 7 are

$$v_1(t,x=x_s) = v_{1,\mathrm{eff}} \tag{11}$$

$$\sigma_{xx}(t,x=x_s) = 0 \tag{12}$$

$$\partial v_1(t,x=0)/\partial x = 0 \tag{13}$$

$$\partial \sigma_{xx}(t,x=0)/\partial x = 0 \tag{14}$$

For the moving boundary position at the solvent–polymer interface, the effects of both solvent swelling and polymer dissolution need to be considered. The effect of solvent swelling can be considered by introducing an

undeformed material coordinate system.[16,17] As solvent diffuses into the polymer, polymer swells or deforms. For one-dimensional diffusion and deformation, the relation between the deformed and the undeformed coordinates is

$$dx = (1 + \epsilon_{xx})\, dX = (1/v_2)\, dX \tag{15}$$

Then, eq 1 can be rewritten as

$$\frac{\partial v_1}{\partial t} = (1 - v_1)\frac{\partial}{\partial X}\left[D_{12}(1 - v_1)\frac{\partial v_1}{\partial X}\right] \tag{16}$$

The initial and boundary conditions are

$$v_1(t=0,X) = 0 \tag{17}$$

$$v_1(t,X=X_s) = v_{1,\text{eff}} \tag{18}$$

$$\partial v_1(t,X=0)/\partial X = 0 \tag{19}$$

where X_s is the moving boundary position at the solvent–polymer interface based on the undeformed coordinate. This term is affected *only by polymer dissolution* but not by solvent swelling.

At the solvent–polymer interface, there is no thermodynamic equilibrium between the solvent and the polymer phases. As a result, the Flory–Huggins theory cannot be used directly to calculate the solvent surface concentration.

As suggested by Papanu et al.,[26] the effective surface concentration can be calculated by considering the change in chemical potential of solvent in the swollen polymer due to the chain entanglements. As the solvent penetrates the polymer, the chains cannot disentangle instantaneously. Thus, there is a resistance to penetration due to the elastic deformation of the entangled polymers and the entangled polymer network behaves like a permanent network so that the Flory–Rehner theory[34] can be applied. The solvent chemical potential in a polymer–solvent mixture is expressed as

$$\mu_1 - \mu_1^0 = \frac{\partial \Delta G_M}{\partial n_1} + \frac{\partial \Delta G_{el}}{\partial n_1} \tag{20}$$

where subscript 1 refers to solvent and subscript 2 to polymer. Here, ΔG_M represents the change of free energy due to mixing which can be expressed in terms of the Flory–Huggins theory, so that

$$\partial \Delta G_M/\partial n_1 = RT[\ln v_1 + (1 - v_1) + \chi(1 - v_1)^2] \tag{21}$$

Also, ΔG_{el} is the change of free energy due to the associated elastic expansion of the polymer matrix, expressed as

$$\Delta G_{el} = \Delta H_{el} - T\delta S_{el} \tag{22}$$

Here, ΔH_{el} and ΔS_{el} represent the change of enthalpy and entropy during chain expansion. According to the rubber elasticity theory, the former is negligible and the latter is equal to

$$\Delta S_{el} = -(k\nu_e/2)[\alpha_z^2 + \alpha_y^2 + \alpha_x^2 - 3 - \ln \alpha_x\alpha_y\alpha_z] \tag{23}$$

where α_x, α_y, and α_z are the expansion factors in three directions and ν_e is the effective number of chains in a network. Since only one-dimensional diffusion and dissolution processes are considered, it is clear that

$$\alpha_y = \alpha_z = 1 \tag{24}$$

and

$$\alpha_x = V/V_0 = 1/(1 - v_1) \tag{25}$$

Here, V/V_0 represents the ratio expansion in the x direction, where V_0 is the unswollen volume in x direction.

Thus, the solvent chemical potential can be calculated from eqs 20–22 as

$$\mu_1 = \mu_1^0 + RT\left[\ln v_1 + (1 - v_1) + \chi(1 - v_1)^2 + \frac{\bar{V}_1}{V_0}\frac{\nu_e}{2N}\left(\frac{2}{v_2} - v_2\right)\right] \tag{26}$$

where the term $\nu_e/2N$ represents the number of moles of cross-links per chain.

The number of moles of cross-links can be replaced by the moles of entanglements per unit value of the polymer, N_e,

$$N_e = (V_0\rho_2/M)\nu_{\text{eff}} \tag{27}$$

Here, ρ_2 is the polymer density, M is the polymer molecular weight, and ν_{eff} is the number of entanglements per polymer molecule which can be approximated by

$$\nu_{\text{eff}} = M/M_e - 1 \tag{28}$$

Finally, M_e is the molecular weight between entanglements, which is estimated from rheological studies,[35]

$$M_e \sim M_c/2 \tag{29}$$

The term M_c is the critical molecular weight of the polymer and can be calculated from the sharp increase in the slope of viscosity vs molecular weight, which is attributed to the onset of entanglements.

Therefore, the chemical potential of the solvent is further expressed from eq 26 as

$$\mu_1 = \mu_1^0 + RT\left[\ln v_1 + (1 - v_1) + \chi(1 - v_1)^2 + \bar{V}_1\rho_2\left(\frac{2}{M_c} - \frac{1}{M}\right)\left(\frac{2}{v_2} - v_2\right)\right] \tag{30}$$

Finally, the effective surface solvent volume fraction, $v_{1,\text{eff}}$, can then be calculated by assuming a quasi-equilibrium between the polymer phase and the pure solvent and by solving the following equation:

$$\ln v_{1,\text{eff}} + (1 - v_{1,\text{eff}}) + \chi(1 - v_{1,\text{eff}})^2 + \bar{V}_1\rho_2\left(\frac{2}{M_c} - \frac{1}{M}\right)\left(\frac{2}{v_{2,\text{eff}}} - v_{2,\text{eff}}\right) = 0 \tag{31}$$

The effect of polymer molecular weight on the effective surface volume fraction is plotted in Figure 2 for the system methyl ethyl ketone/polystyrene, when M_c is 38 000, a typical critical molecular weight for polystyrene,[39] and $\chi_1 = 0.49$. It can be seen that, in the low molecular weight region, $v_{1,\text{eff}}$ decreases with increasing polymer molecular weight. It then levels off and reaches a constant value when the polymer molecular weight is above 200 000.

Polymer Dissolution Model. As solvent molecules continuously diffuse into a glassy polymer, the local polymer glass transition temperature decreases. When the solvent volume fraction reaches a critical solvent volume fraction for gel formation, $v_{1,g}$, the glassy transition temperature is lowered to the experimental temperature and the original glassy layer becomes rubbery. Long-range cooperative motion of chains that would result in trans-

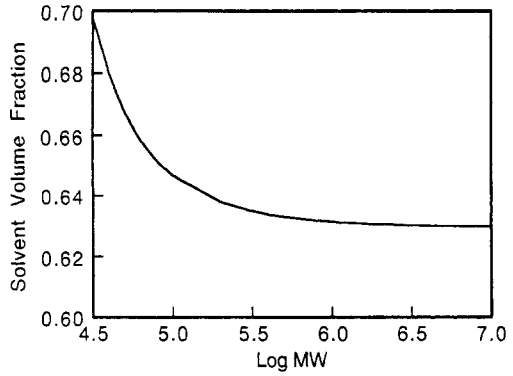

Figure 2. Effective MEK surface volume fraction as a function of polystyrene molecular weight. The curve was calculated from eq 31 with MEK/polystyrene $\chi = 0.49$ and a critical molecular weight of polystyrene[39] of $M_c = 38\,000$.

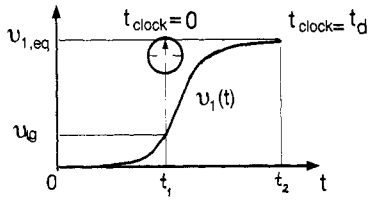

Figure 3. Solvent volume fraction history at a spatial point. When the solvent volume fraction is equal to the critical gel volume fraction, $v_{1,g}$, the dissolution clock starts, t_1. When the clock time, t_2, is equal to the disentanglement time, t_d, the polymer at this point is dissolved.

lational motions of molecules is still greatly restricted by the presence of strong local interactions between neighboring chains. Nevertheless, short-range diffusion motions of polymer segments occur, resulting in the disentanglement of polymer chains.

The disentanglement of a polymer chain can be described by its diffusion through a tube, which follows the shape of the chain. In polymer dissolution, a polymer chain needs a period of time to complete a movement from the entanglement rubbery state to the dissolved liquid state. It is reasonable to consider that a chain is in an entangled state when it is trapped in a tube; it changes to a disentangled state when it diffuses out of its tube. The time required for this process is the disentanglement time, henceforth designated as t_d. It may be considered as a characteristic time for the dissolution process. At each point in a polymer sample, disentanglement starts when the solvent concentration at this point reaches the critical gel concentration. After a period of time equal to the disentanglement time, the polymer molecules at this point are dissolved. It is instructive to introduce the concept of dissolution clock to describe the dissolution process. This idea originated in polymer viscoelasticity[37-39] to describe relaxational behavior of polymers. Initially, a dissolution clock is set to be zero at each point in a polymer sample. The clock measures time only after the solvent concentration at a point reaches the critical gel concentration. Thus, the clocks at different positions may start at different times because of the nonuniform concentration distribution. After the clock time at a point is equal to the disentanglement time, the polymer at that point is dissolved (see also Figure 3).

An expression for the reptation time can be derived from the reptation theory and the resultant scaling laws.[40-42] The reptation time[43] scales to

$$t_R \sim L_t^2/D_{tube} \tag{32}$$

where L_t is the tube length and D_{tube} is the tube diffusion coefficient. The tube length is proportional to the number of entanglement units per tube and the distance between entanglements. Thus,

$$L_t \sim (M/g)\xi \tag{33}$$

In this expression, M is the polymer molecular weight and g is the number of monomer units in an entanglement subunit, which can be expressed as

$$g \sim v_2\xi^3 \tag{34}$$

Here, ξ is the distance between entanglements, which is independent of polymer molecular weight, but related to polymer concentration. In general, we may write

$$\xi \sim v_2^{-a} \tag{35}$$

with the exponent a becoming 0.75 for good solvents and 1.0 for Θ solvents. Thus, L_t scales to

$$L_t \sim M v_2^{2a-1} \tag{36}$$

The tube diffusion coefficient can be expressed as

$$D_{tube} \sim kT\mu_t \tag{37}$$

Here, μ_t is the polymer chain mobility, which is inversely proportional to the number of entanglement units,

$$\mu_t \sim \mu_1(g/M) \tag{38}$$

where μ_1 is the mobility of an entanglement unit, which is expressed as

$$\mu_1 \sim 1/\eta_s\xi \tag{39}$$

where η_s is solvent viscosity. Therefore, the tube diffusion coefficient scales to

$$D_{tube} \sim (kT/\eta_s\xi)(g/M) \tag{40}$$

$$D_{tube} \sim (kT/\eta_s)M^{-1}v_2^{1-2a} \tag{41}$$

By substituting eqs 36 and 41 into eq 32, we obtain

$$t_R \sim (\eta_s/kT)M^{3.0}v_2^{6a-3} \tag{42}$$

The reptation time may be expressed for good solvents ($a = 0.75$) as

$$t_R \sim (\eta_s/kT)M^{3.0}v_2^{1.5} \tag{43}$$

Since neither the tube diffusion coefficient nor the reptation time are directly measurable, the above scaling laws can be tested by measuring the polymer self-diffusion coefficient, which can be expressed in terms of the radius of gyration and the reptation time, that is

$$D_{self} \sim R_g^2/t_R \tag{44}$$

Since

$$R_g \sim (M/g)^{0.5}\xi \tag{45}$$

the scaling expression for the self-diffusion coefficient becomes

$$D_{self} \sim M^{-2.0}v_2^{2-5a} \tag{46}$$

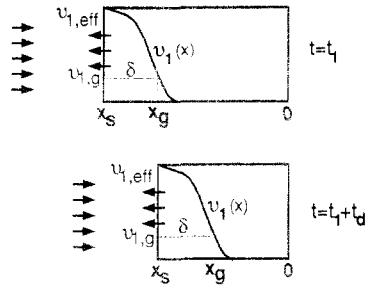

Figure 4. Moving positions of the solvent–polymer and the gel–glassy interfaces. (a) At time t_1, the solvent volume fraction at the gel–glassy interface, x_g, is equal to $v_{1,g}$ and the dissolution clock at this position starts to measure time; (b) after a time period of t_d, the dissolution clock time at $x_g(t_1)$ is equal to the disentanglement time so that the polymer at this position is dissolved. Both interface positions travel a distance δ, which is the gel layer thickness.

For good solvents,

$$D_{self} \sim M^{2.0} v_2^{-1.75} \tag{47}$$

This relation has been verified experimentally.[44,45]

It is important to note that the scaling laws of the reptation theory describe the movement of a single linear chain in an identical polymer matrix. The disentanglement occurring during polymer dissolution may be different from the self-diffusion of a single chain because the solvent concentration (volume fraction) is not uniform in the gel layer so that the polymer concentration gradient may play a role in the chain disentanglement. Since the disentanglement time can also be defined as a delay time, the effect of a concentration gradient on polymer dissolution is to reduce the delay time. Because of the existence of a concentration gradient, the molecular weight dependence in a dissolution process can be expected to be lower than that predicted by the reptation theory. Moreover, the concentration dependence of the disentanglement may also differ from that expected by the reptation theory because the disentanglement occurs in a wide concentration (volume fraction) range, from the solvent critical gel concentration to the solvent effective surface concentration.

To differentiate the disentanglement time for polymer dissolution from the reptation time for self-diffusion, a general expression for the disentanglement time is preferred here:

$$t_d^0 = k_d M^\alpha v_2^\beta \tag{48}$$

Here, t_d^0 is the disentanglement time at a constant volume fraction level and k_d is a disentanglement time constant.

The disentanglement time calculated from eq 48 can be used only if the solvent volume fraction during the entire disentanglement process is constant. As the solvent volume fraction at any point inside a polymer changes continuously during a dissolution process, as shown in Figure 4, the solvent volume fraction changes from the critical gel to the effective surface volume fraction. The solvent volume fraction reaches $v_{1,g}$ at time t_1, whereas the polymer molecules dissolve at t_2. Thus, the disentanglement time required, t_d, is $t_2 - t_1$. The fractional contribution of the differential time interval (at concentration $v_{1,i}$) to the disentanglement is

$$f_{d,i} = \Delta t_i / t_d^0(v_{1,i}) \tag{49}$$

with their sum equal to unity as i approaches infinity. Thus, from eqs 48 and 49 we obtain

$$\int_{t_1}^{t_2} \frac{dt}{k_d M^\alpha v_2^\beta} = 1 \tag{50}$$

Since k_d and M are independent of time, the above equation can be written as

$$t_d = k_d M^\alpha \overline{v_2^\beta} \tag{51}$$

where

$$\overline{v_2^\beta} = 1/\left(\frac{1}{t_2 - t_1}\int_{t_1}^{t_2} \frac{dt}{v_2^\beta}\right) \tag{52}$$

As the effective v_2^β is an average, there is an implicit dependence on v_2. In the case that the solvent volume fraction gradient in the gel layer is very small, there is a distinct transition at the gel–glassy interface, the solvent volume fraction during a disentanglement process is almost constant, and the disentanglement time can be approximately calculated by

$$t_d = k_d M^\alpha v_{2,eff}^\beta \tag{53}$$

For a polymer sample as shown in Figure 4, one-dimensional diffusion and dissolution occurs. At time t_1, the volume fraction profile is $v_1(\chi,t_1)$. At the gel–glassy interface x_g, the solvent volume fraction is equal to $v_{1,g}$ and the dissolution clock is zero. After a time period of t_d, the dissolution clock time at $x_g(t_1)$ is equal to the disentanglement time so that the polymer at this position is dissolved. The resultant boundary position and volume fraction profile are shown in Figure 4 at $t = t_1 + t_d$. During this period of time, the solvent volume fraction front moves a distance of δ, which is equal to the thickness of the gel layer. As a result, we can write

$$t_d \sim \delta^2 / D_{12} \tag{54}$$

By substituting eq 51 into eq 54 and assuming that the diffusion coefficient is independent of polymer molecular weight, a scaling law for the dependence of the gel layer thickness on polymer molecular weight can be obtained as

$$\delta \sim M^{\alpha/2} \tag{55}$$

A scaling law can also be obtained for the dissolution rate as

$$R_d \sim \frac{\delta}{t_d} \sim \frac{M^{\alpha/2}}{M^\alpha} \sim M^{-\alpha/2} \tag{56}$$

Obviously, the disentanglement time can be regarded as the characteristic dissolution time whereas the ratio of the characteristic dissolution time to the characteristic diffusion time can be defined as the *dissolution number*, or D_s.

$$D_s = t_d / \tau_{dif} \tag{57}$$

Here, τ_{dif} is the characteristic diffusion time, which is defined as L_0^2/D_{12}. Thus, we can further obtain

$$D_s = t_d D_{12} / L_0^2 \sim \delta^2 / L_0^2 \tag{58}$$

The above scaling result indicates that the square of the gel layer thickness scales to the relative magnitude of the characteristic polymer disentanglement time to the characteristic solvent diffusion time, or to the dissolution

number. The dissolution number is useful only if the solvent penetration is controlled by solvent diffusion.

If the solvent penetration is controlled by the polymer relaxation, we can define a *modified dissolution number*, D'_s

$$D'_s = D_s/De = t_d/\tau_{relax} \tag{59}$$

where De is the diffusion Deborah number, which is defined as the ratio of the characteristic polymer relaxation time to the characteristic solvent diffusion time.[46] If D_s or D'_s is greater than 1, the polymer dissolution rate is lower than the solvent penetration rate, resulting in a thick gel layer. If D_s or D'_s is lower than 1, the dissolution rate is faster than the solvent penetration rate rate, yielding a thin gel layer.

Numerical Solution. The complete dissolution model required simultaneous solution of the solvent transport and polymer disentanglement equations.

A finite difference scheme was used to solve eqs 1–4 when Fickian solvent diffusion occurs. For Fickian solvent diffusion behavior, eqs 6–14 were solved with the numerical algorithm we have presented elsewhere.[47]

The numerical scheme used in this work for simulating polymer dissolution was the same as that without dissolution,[47] except that each spatial grid point was assigned a dissolution clock and the polymer molecules whose clock time was greater than the disentanglement time were eliminated. This resulted in a moving boundary which was controlled by the disentanglement model.

The following numerical procedure was used to implement the finite difference scheme of ref 47.

(1) At each time step, the concentrations at all spatial grid points were checked. If the solvent concentration at a point was greater than the critical gel concentration, the dissolution clock was started at this point.

(2) At each time step, all the fractional contributions to the disentanglement time as defined in eq 49 were checked. If the clock time at a point was equal to the critical disentanglement time, the boundary condition was moved to this point. The moving boundary position at the solvent–polymer interface based on undeformed coordinate, X_s, was determined by

$$X_s = (i/n)L_0 \qquad i = 1, 2, ..., n \tag{60}$$

where n is the total number of spatial grids before dissolution, i is the current number of spatial grids controlled by the dissolution clock at each grid point, and L_0 is the half-thickness of the polymer. The dimensionless boundary position based on the undeformed coordinate is

$$\bar{S}/\bar{X}_s = X_s/L_0 \tag{61}$$

(3) The actual moving boundary position at the solvent–polymer interface was obtained by using the deformed coordinate as follows:

$$x_s = \int_0^{X_s}(1 + \epsilon_{xx})\,dX = \int_0^{X_s}\frac{1}{1-\upsilon_1}\,dX \tag{62}$$

The dimensionless boundary position based on the deformed coordinate is

$$\bar{x}_s = x_s/L_0 \tag{63}$$

(4) The actual moving boundary position at the gel–glassy interface, x_g, was determined as follows:

$$x_g = \int_0^{X_g}(1 + \epsilon_{xx})\,dX = \int_0^{X_g}\frac{1}{1-\upsilon_1}\,dX \tag{64}$$

Here, X_g is the moving boundary position at the gel–glassy interface based on undeformed coordinates.

(5) The dimensionless gel layer thickness was determined by

$$\bar{\delta} = (x_s - x_g)/L_0 \tag{65}$$

(6) The polymer dissolution rate was calculated by taking the slope of x_s vs time data:

$$R_d = -(dx_s/dt) \tag{66}$$

Experimentally, R_d can be obtained by measuring the change of the thickness of the polymer film in a dynamic dissolution process. The dimensionless dissolution rate in terms of the moving boundary position was

$$\bar{R}_d = -(d\bar{x}_s/d\theta) \tag{67}$$

where θ is a dimensionless time defined as

$$\theta = \frac{t}{\tau_{dif,\upsilon_{1,eff}}} = \frac{tD_0\exp(a_d\upsilon_{1,eff})}{L_0^2} \tag{68}$$

The polymer dissolution rate could also be calculated in terms of the mass change of a polymer, designated as R_m.

$$R_m = -(dM_p/dt) = -A\rho_2(dX_s/dt) \tag{69}$$

Here, M_p is the mass of polymer and A is the cross section of the polymer sample. This dissolution rate could be obtained by taking the slope of X_s vs time data or measured by the mass change of a polymer sample. Finally, the dimensionless dissolution rate was expressed as

$$\bar{R}_m = -(d\bar{X}_s/d\theta) \tag{70}$$

Experimental Section

Preparation of Polymer Samples. Two polymers were used in the present work, polystyrene and poly(methyl methacrylate) (PMMA). Polystyrene grades had $\bar{M}_n$ of 28 000 (PI = 1.06), 56 000 (PI = 1.04), 107 000 (PI = 1.02), 380 000 (PI = 1.06), and 620 000 (PI = 1.06), all (obtained from Polysciences, Inc., Warrington, PA), $\bar{M}_n$ of 890 000 (PI = 1.06, Aldrich Chemical Co., Milwaukee, WI), $\bar{M}_n$ = 1 260 000 (PI = 1.13, Aldrich Chemical Co.), $\bar{M}_n$ = 1 520 000 (PI = 1.30, Scientific Polymer Products, Inc., Ontario, NY), and $\bar{M}_n$ = 2 830 000 (PI = 1.06, Polysciences). Polystyrene films were prepared by molding at 140 °C for 3 h and 150 °C for 6 h at 92 MPa.

PMMA films were prepared by polymerization of vacuum distilled MMA with 0.2 wt % benzoyl peroxide at 60 °C for 50 min. The reaction medium was then poured into a special mold and further reacted at 60 °C for 48 h and 90 °C for 24 h.

Sorption Experiments. Polystyrene samples produced by the previous techniques were cut into specimens of 35 mm × 15 mm × 1 mm. They were placed in vials containing methyl ethyl ketone (MEK) at 27 °C, and gravimetric studies were performed to determine their dynamic swelling behavior. Selected samples were immersed in a MEK/poly(ethylene glycol) (PEG 400, molecular weight 400, Aldrich, Milwaukee, WI) solution containing 43 vol % MEK.

Pulsed-Gradient Spin-Echo NMR Experiments. The self-diffusion coefficient of MEK in polystyrene was measured using spin-echo NMR spectroscopy. Thin-wall NMR tubes (7 mm o.d., 6 mm i.d., 225 mm long, Pyrex precision bore, made by Wilmal Glass Co., Buena, NJ) were filled with polystyrene of average molecular weight 180 000 (Polysciences, Inc., Warrington, PA) and known concentration. MEK was then added so that the

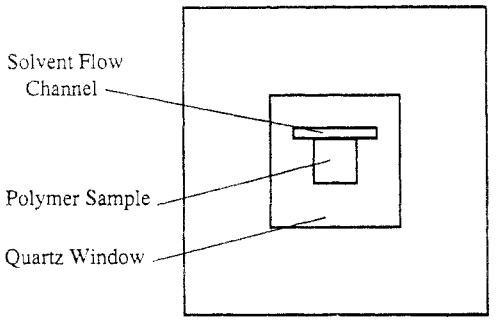

Figure 5. Schematic diagram of the dissolution call, which is mounted on the critical angle illumination microscope.

total height of the polymer–solvent mixture in the tubes was 9 mm. The sample tubes were then placed into a liquid nitrogen bath to prevent MEK evaporation, and the tubes were sealed under vacuum. They were then placed in an oven at 65 °C for 2 months. Experimental results showed that was a sufficient time for the polymer–solvent mixtures to yield a uniform solvent concentration. In a typical NMR experiment, a sample tube was placed into a magnetic field chamber at the desired temperature. The duration of the gradient pulses was changed sequentially and the spin-echo intensity was recorded.

Dissolution Experiments. A critical angle illumination microscope was built to measure the polymer dissolution rate and the gel layer thickness. The microscope was adapted from a goniometer (Model 100-00, Rame-Hart, Inc., Mountain Lakes, NJ) and was equipped with a custom-made sample cell and a solvent pumping system (Spectroflow 400, Ramsey, NJ). Figure 5 shows a schematic diagram of the sample cell. It was composed of a housing that was made of Kel-F and a pair of quartz windows (Quartz Scientific, Inc., Fairport Harbor, OH). One of the windows was tapped with two holes to allow solvent to flow in and out of the sample cell. A Teflon spacer was used to hold the polymer sample so that only one side of the sample was exposed to the solvent. The sample cell was mounted on the movable x–y stage of the goniometer, which could be adjusted vertically in 0.01 mm increments.

Polystyrene and PMMA samples were cut with a sharp knife (5×5 mm^2) to fit in the rectangular slot of the Teflon spacer. Exact fitting was achieved by polishing the cut samples with 360-A silicon carbide sand paper. A multipurpose sealant (Dow Corning 732, Midland, MI) was used to seal the tiny gap between the polymer sample and the Teflon spacer. The illuminating light was from a xenon source with a green narrow-pass band filter which was mounted on a goniometer, allowing the angle of illumination to vary from 0 to 20°. Since the goniometer was mounted on a rail, the distance between the sample and the light source could also be varied. The microscope (×22) was used to monitor polymer dissolution. A video camera was connected to the microscope, and the dissolution process was followed on a color monitor and was recorded. The solvent–gel and gel–glassy interface positions could be read directly from the screen. The accuracy of the first method was about 0.01 mm, leading to an experimental error of 0.1% in any measured interface position. In all the dissolution experiments, the solvent flow rate was fixed at 0.3 mL/min.

Results and Discussion

Solution of the Mathematical Model. The new mathematical model was first solved for the case of polystyrene dissolution in MEK, which exhibited swelling and polymer disentanglement. For this purpose, several parameters were calculated by use of standard physicochemical values for this system.

The MEK surface volume fraction, $v_{1,\text{eff}}$, was calculated from eq 31. Here, the MEK/polystyrene interaction parameter,[16] χ, was 0.49, the molar volume of MEK was $\bar{v}_1 = 89.4$ cm^3/mol calculated as $\bar{v}_1 = M_1/\rho_1 = 72/0.805$ cm^3/mol, the polystyrene density was $\rho_2 = 1.05$ g/cm^3, the critical molecular weight of polystyrene[39] was $M_c = 38\,000$,

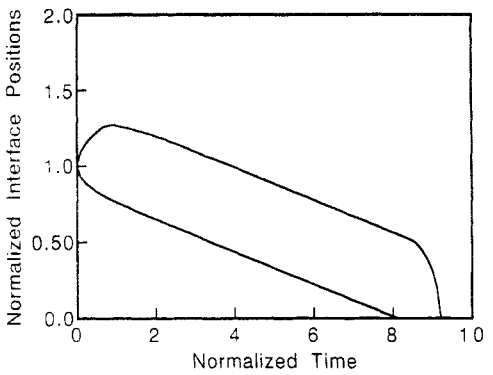

Figure 6. Numerical predictions of the interface positions normalized with respect to the half-thickness, L_0, as functions of dimensionless time during dissolution of polystyrene in MEK. The upper curve represents the solvent–gel interface while the lower curve represents the gel–glassy interface position. The parameters used in the simulation were $L_0 = 0.01$ cm, $M = 400\,000$, $M_c = 38\,000$, $\chi = 0.49$, $D_0 = 1.1 \times 10^{-10}$ cm^2/s, $a_d = 20$, $k_d = 2.15 \times 10^{-4}$ s, $\alpha = 2$, and $\beta = 12$.

and the value of M was the $\bar{M}_n$ of the polystyrene sample used in the studies (see Experimental Section).

Parameters affecting the MEK diffusion were the preexponential factor of the MEK diffusion coefficient, D_0 (see eq 5), the exponential factor, a_d, and the half-thickness of the polymer film, $L_0 = 0.01$ cm. MEK self-diffusion coefficient data obtained by NMR experiments indicated that the mutual diffusion coefficient at zero solvent concentration, D_0, was 1.1×10^{-10} cm^2/s. The exponent of the volume fraction dependence of the diffusion coefficient, a_d, was 20 so that the MEK diffusion coefficient was about 10^{-6} cm^2/s at the MEK volume fraction of $v_1 = 0.5$. This value is consistent with the data used by Tu and Ouano.[24]

Other parameters used in the simulation of polymer dissolution were the disentanglement time constant, $k_d = 2.15 \times 10^{-4}$ s, the exponential factors for molecular weight, $\alpha = 2$, and volume fraction, $\beta = 12$, and the critical gel volume fraction, $v_{1,g} = 0.18$.

Various simulations and solutions of the mathematical model were performed in order to investigate the influence of various parameters on polystyrene dissolution. First, the importance of polystyrene molecular weight on polymer dissolution was examined by determining the front positions, x_g and x_s, the gel thickness δ, the polystyrene mass loss, and the MEK volume fraction profile as functions of time. In the simulations and results presented in Figures 6–9, the effective MEK surface volume fraction and the MEK diffusion coefficient were kept constant.

Figure 6 shows the MEK front positions in polystyrene slabs of molecular weight of $M = 400\,000$ as functions of dissolution time. These are the normalized positions of the liquid–gel (upper curve) and gel–glassy (lower curve) interfaces. There are three distinct dissolution stages. During the early stage, MEK diffuses into polystyrene and the sample swells without dissolution. After an induction time, dissolution is exhibited which reaches a stationary phase. In this stage, the gel layer thickness becomes constant; i.e., the two fronts are parallel. At the end of the stationary stage, the gel–glassy interface disappears and the liquid–gel interface moves rapidly toward the center until the polystyrene sample is completely dissolved. This acceleration in the dissolution rate can be attributed to the higher MEK volume fraction at the final dissolution stage, which gives rise to a shorter disentanglement time. The three dissolution steps or stages could be distinguished clearly when the normalized thickness of the gel layer was plotted vs the dimensionless

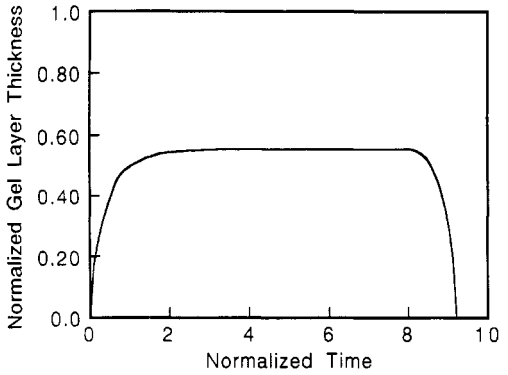

Figure 7. Numerical predictions of the normalized gel layer thickness as a function of dimensionless time for polystyrene dissolution in MEK, using the same parameters as in Figure 6.

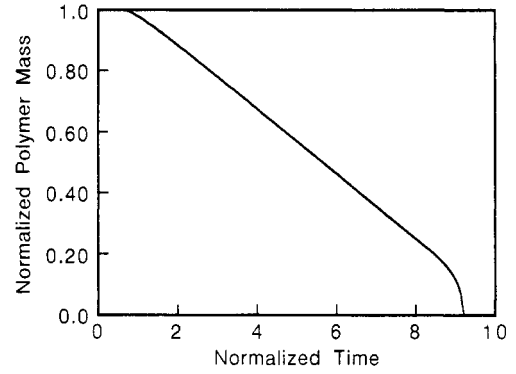

Figure 8. Numerical predictions of the normalized polystyrene mass loss as a function of dimensionless time for polystyrene dissolution in MEK using the same parameters as in Figure 6.

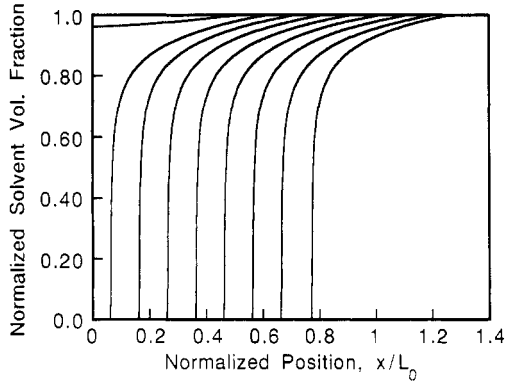

Figure 9. Numerical predictions of the normalized MEK volume fraction as a function of normalized position for polystyrene dissolution in MEK using the same parameters as in Figure 6. The dimensionless time increases by $\Delta\theta = 0.94$ starting from the right to the left.

time, as in Figure 7. Clearly, swelling predominates during the early portion of the process when the gel layer thickness increases with time. This is followed by a period of front synchronization when the normalized gel thickness remains constant due to equal swelling and dissolution. In the last stage of process, the gel thickness decreases with time.

The ratio of polystyrene mass at time t to that at time 0 was plotted vs time in Figure 8. The constant gel thickness stage of Figure 7 corresponded to the constant weight loss section of Figure 8 observed between $\theta_1 = 0.9$ and $\theta_2 = 8.9$. Finally, the volume fraction profile of MEK in the polystyrene slab is shown in Figure 9 for different times. The shapes of these curves indicate the stationary stage of dissolution, with front profiles moving at constant velocity.

The effect of molecular weight on polymer dissolution was studied by plotting the normalized position of the two

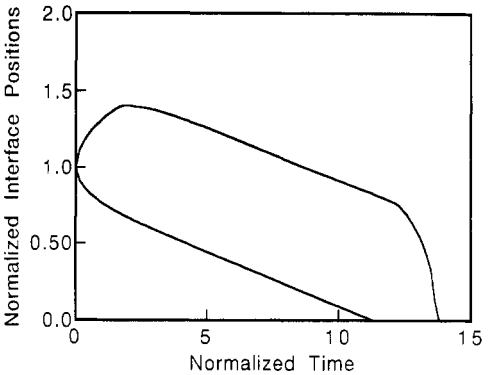

Figure 10. Numerical predictions of the interface positions normalized with respect to the half-thickness, L_0, as functions of dimensionless time during dissolution of polystyrene in MEK. The upper curve represents the solvent–gel interface while the lower curve represents the gel–glassy interface position. The parameters used in the simulation were $L_0 = 0.01$ cm, $M = 600\,000$, $M_c = 38\,000$, $\chi = 0.49$, $D_0 = 1.1 \times 10^{-10}$ cm^2/s, $a_d = 20$, $k_d = 2.15 \times 10^{-4}$ s, $\alpha = 2$, and $\beta = 12$.

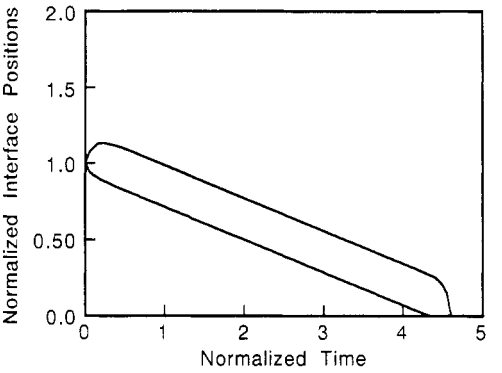

Figure 11. Numerical predictions of the interface positions normalized with respect to the half-thickness, L_0, as functions of dimensionless time during dissolution of polystyrene in MEK. The upper curve represents the solvent–gel interface while the lower curve represents the gel–glassy interface position. The parameters used in the simulation were $L_0 = 0.01$ cm, $M = 200\,000$, $M_c = 38\,000$, $\chi = 0.49$, $D_0 = 1.1 \times 10^{-10}$ cm^2/s, $a_d = 20$, $k_d = 2.15 \times 10^{-4}$ s, $\alpha = 2$, and $\beta = 12$.

fronts as a function of time for different polystyrene molecular weights. Figure 10 shows the simulation for polystyrene dissolution by MEK, when the polystyrene molecular weight is 600 000. These data should be compared to those of Figure 6. It can be seen that the thickness of the gel layer, i.e., the difference of front positions at a specific time, increases significantly as the molecular weight increases from 400 000 to 800 000. This is attributed to the longer disentanglement time caused by the larger molecular weight, and is consistent with the dissolution number defined in eq 58, which is the ratio of the characteristic disentanglement time to the characteristic diffusion time. As the disentanglement time and the dissolution number increase, the thickness of the gel layer increases. Simulation results for polystyrene molecular weight decreasing from 400 000 to 200 000 are shown in Figure 11. Clearly, the gel layer thickness decreases significantly as the molecular weight decreases.

As shown by eq 65, the thickness of the gel layer during dissolution is a function of the polystyrene molecular weight and depends on the value of the exponent α. Figure 12 presents theoretical results of the logarithm of the gel layer thickness, δ, normalized with respect to the initial half-thickness of the film, L_0, and plotted vs the logarithm of the polystyrene molecular weight for values of α of 1, 2, or 3. The three slopes are 0.5, 1.0, and 1.5, respectively, consistent with the analysis of eq 55. Using the same

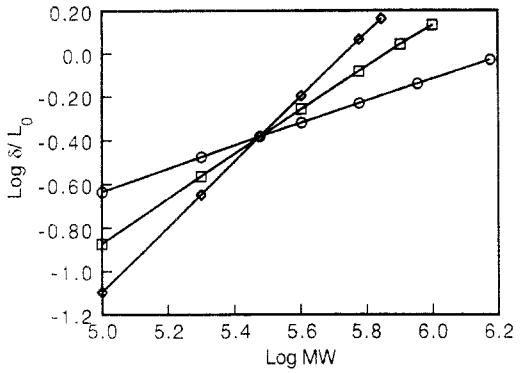

Figure 12. Numerical prediction of the influence of polystyrene molecular weight on normalized gel layer thickness for polystyrene dissolution in MEK using different values of the exponent α of eq 55 of α = 1 (○), 2 (□), and 3 (◇). The parameters used in the simulation were L_0 = 0.01 cm, M_c = 38 000, χ = 0.49, D_0 = 1.1 × 10^{-10} cm^2/s, a_d = 20, k_d = 2.15 × 10^{-4} s, α = 2, and β = 12.

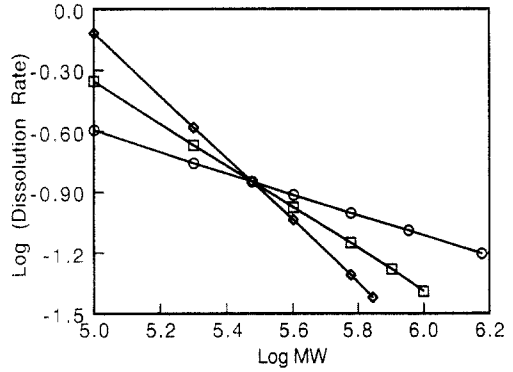

Figure 13. Numerical prediction of the influence of polystyrene molecular weight on the normalized polymer dissolution rate for polystyrene dissolution in MEK using different values of the exponent α of eq 56 of α = 1 (○), 2 (□), and 3 (◇). The parameters used in the simulation were L_0 = 0.01 cm, M_c = 38 000, χ = 0.49, D_0 = 1.1 × 10^{-10} cm^2/s, a_d = 20, k_d = 2.15 × 10^{-4} s, α = 2, and β = 12.

simulations, the dimensionless mass dissolution rate was calculated and plotted in Figure 13 as a function of polystyrene molecular weight. The slopes of the three lines are −0.5, −1.0, and −1.5, respectively.

In the above simulations, the exponential factor of concentration dependence of the disentanglement time, β, was kept constant. The effect of β on the disentanglement time is clearly understood by the following process. During a dynamic dissolution process, the solvent volume fraction at a fixed spatial point varies significantly with time. Suppose that dissolution occurs at two different volume fractions, $v_{2,1}$ and $v_{2,2}$. The disentanglement times at the two volume fraction values are

$$t_{d,1} = k_d M^{\alpha} {v_{2,1}}^{\beta} \tag{71}$$

$$t_{d,2} = k_d M^{\alpha} {v_{2,2}}^{\beta} \tag{72}$$

For the same polystyrene samples, k_d and M are the same. Thus,

$$t_{d,1}/t_{d,2} = [v_{2,1}/v_{2,2}]^{\beta} \tag{73}$$

Assume that

$$v_{2,1} = 0.8 \quad \text{or} \quad v_{1,1} = 0.2 \tag{74}$$

and

$$v_{2,2} = 0.4 \quad \text{or} \quad v_{1,2} = 0.6 \tag{75}$$

The MEK volume fraction of 0.2 is very close to the critical gel volume fraction where polystyrene still passes a transition from the glassy to the rubbery state. The MEK volume fraction of 0.6 is close to the effective surface volume fraction where the polymer is in a transition from the rubbery to liquid state. By substituting the two values into eq 73, we obtain

$$t_{d,1}/t_{d,2} = 2^{\beta} \tag{76}$$

From the scaling law, it is known that β is equal to 1.5 for good solvents and to 3.0 for Θ solvents. However, experimental results have shown that these values are valid only in dilute or semiconcentrated regions. As a solution becomes more and more concentrated, β becomes larger than 3.0.[45] For dissolution of a glassy polymer, the disentanglement occurs in a wide range within the concentrated solution region. It can be expected that the disentanglement time at the gel–liquid interface is significantly different from that at the gel–glassy interface. According to eq 76, if β is 3, the disentanglement time at the gel–glassy interface is just about 1 order of magnitude longer than that at the MEK–gel interface, an unreasonable conclusion. If β is increased to 6, the disentanglement time at the gel–glassy interface is just about 2 orders of magnitude longer than that at the MEK–gel interface.

The effect of β on the dissolution behavior is shown in Figure 14, which can be compared to Figure 6. For β equal to 6, the dissolution simulations indicate that there is a relatively sharp transition from the initial stage to the stationary stage (see Figure 14). This is because the disentanglement times at different concentration levels are quite close. For β equal to 12, the transitions becomes quite smooth, as shown in Figure 6. It should be noted that the value of β is related to the term a_d of the MEK diffusion coefficient defined in eq 5. The larger the a_d, the more appreciable is the MEK volume fraction change during dissolution and a larger value of β is needed.

Sorption Experimental Observations. In order to investigate MEK diffusion in polystyrene without dissolution, it was necessary to lower the MEK activity. For the MEK/polystyrene system, poly(ethylene glycol) (MW = 400) (PEG 400) was used as an additional diluent since it is miscible with MEK in all concentrations while incompatible with polystyrene. For example, a thin polystyrene film placed in PEG 400 for three months at 75 °C did not show any weight change.

Investigation of the dynamic swelling behavior of polystyrene samples was conducted in a 43 vol % MEK solution. Typical MEK uptake curves as a function of time are shown in Figure 15 for four polystyrene samples with molecular weights $\bar{M}_n$ of 28 000, 56 000, 107 000, and 620 000. A simple empirical equation was used to analyze the MEK transport behavior.

$$M_t/M_\infty = kt^n \tag{77}$$

Here, M_t is the MEK uptake at time t and M_∞ is the MEK uptake after equilibrium swelling. If n is 0.5, the solvent transport is Fickian. If n is 1.0, the solvent transport is case II.[48] By fitting the first 10 data points on each curve using the above equation, the resultant values of n were 0.49, 0.50, 0.54, and 0.55 for MEK transport in polystyrene film of molecular weights 28 000, 56 000, 107 000, and 620 000, respectively. For all four samples, the 95% confidence intervals of n were less than ±0.05. Thus, the dynamic swelling process was Fickian since n was close to

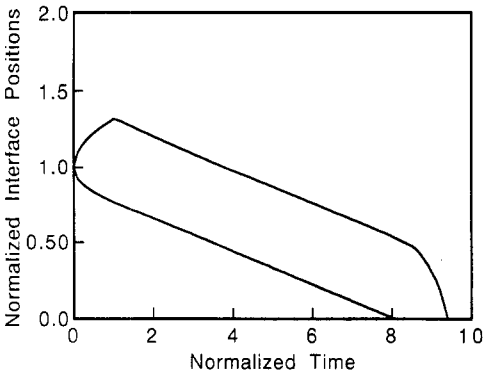

Figure 14. Numerical predictions of the interface positions normalized with respect to the half-thickness, L_0, as functions of dimensionless time during dissolution of polystyrene in MEK. The upper curve represents the solvent–gel interface while the lower curve represents the gel–glassy interface position. The parameters used in the simulation were $L_0 = 0.01$ cm, $M = 400\,000$, $M_c = 38\,000$, $\chi = 0.49$, $D_0 = 1.1 \times 10^{-10}$ cm^2/s, $a_d = 20$, $k_d = 2.15 \times 10^{-4}$ s, $\alpha = 2$, and $\beta = 6$.

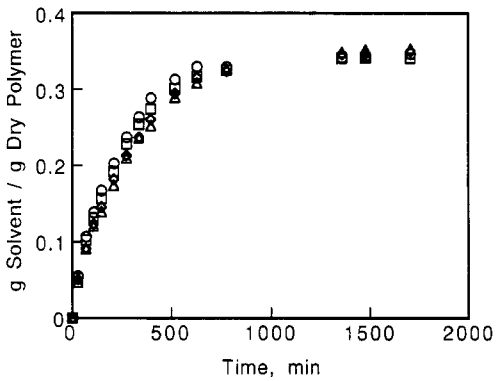

Figure 15. MEK uptake in polystyrene at 27 °C from PEG 400/MEK solution containing 43 vol % MEK. The polystyrene molecular weights were 28 000 (○), 56 000 (□), 107 000 (◇), and 620 000 (△).

0.5 for all four cases. At equilibrium, all samples were in rubbery state.

Before further analysis of these results, the dependence of the MEK self-diffusion coefficient on MEK concentration (volume fraction) was investigated using pulsed-gradient spin-echo NMR experiments[49] in order to ascertain whether any deviations from Fickian behavior were the result of such a concentration dependence. Ten polystyrene samples containing MEK in volume fractions of 0.21, 0.25, 0.27, 0.30, 0.36, 0.40, 0.47, 0.59, 0.71, and 1.0 were used.

The MEK self-diffusion coefficient was determined at 30 and 40 °C as described before[49] and plotted against MEK volume fraction, as seen in Figure 16. The concentration (volume fraction) dependence of the self-diffusion coefficient was significant in the low MEK concentration region. Third-order polynomials were used to fit the data at each temperature. The resulting polynomial for the data at 40 °C was

$$\ln D_1 = -10.07 + 20.82v_1 - 28.43\,v_1^2 + 13.35v_1^3 \quad (78)$$

The polynomial for the data at 30 °C was

$$\ln D_1 = -9.62 + 17.13v_1 - 21.26v_1^2 + 9.26v_1^3 \quad (79)$$

The correlation coefficients for the both polynomials were higher than 0.999.

Experimental Observations of the Dissolution Process. Dissolution experiments with the critical angle

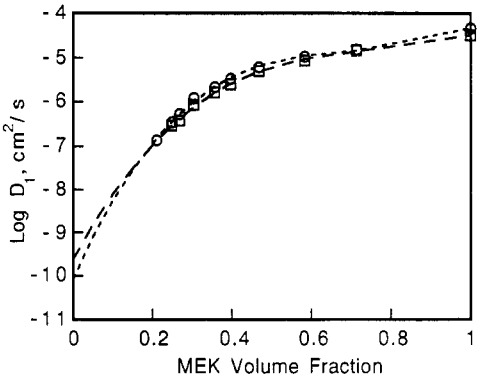

Figure 16. MEK self-diffusion coefficient in polystyrene measured by pulsed-gradient spin-echo NMR spectroscopy as a function of MEK volume fraction at 40 (○) and 30 °C (□).

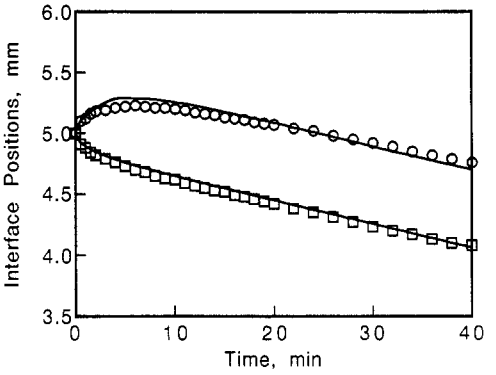

Figure 17. MEK–gel (○) and gel–glassy polystyrene (□) interface positions as a function of time during monodisperse polystyrene dissolution ($\bar{M}_n = 380\,000$) in MEK at 27 °C. The curves represent the prediction of the mathematical model.

illumination microscope were conducted in two modes. Typically, MEK was passed on top of the polystyrene samples. It was observed that after MEK was in contact with a polystyrene sample, the gel–glassy interface moved downward gradually, while the solvent–gel interface moved upward. The gel layer thickness increased continuously even after a relatively long period of time. No stationary dissolution stage was observed. These observations are quite similar to those by Tu and Ouano[24] and are related to the density difference between polystyrene and MEK.

To overcome this problem, MEK was allowed to flow parallel to the lower surface of the polystyrene film. In this way, the dissolved polystyrene was quickly mixed with MEK and washed out of the sample cell. As a result, after an initial stage in which the polymer sample swelled, a stationary dissolution stage was obtained with both the solvent–gel and the gel–glassy interfaces moving at the same velocity, giving rise to a constant gel layer thickness. The effect of polymer molecular weight on the gel layer thickness was investigated by dissolving monodisperse polystyrene samples in MEK. Figures 17–19 show the solvent–gel and gel–glassy interface positions as functions of time for three different polymer molecular weights. In these figures, the upper curves represent the position of the solvent–polymer or solvent–gel interface as a function of time whereas the lower curves represent the position of the gel–glassy interface. Before the dissolution process, the polymer boundary position was at 5 mm. At the beginning of the dissolution process, the polymer boundary position was at 5 mm. At the beginning of the dissolution process, the polystyrene began to swell and an induction time was observed before a polymer started dissolving. This time depended upon the polymer molecular weight. After a period of time, the dissolution became stationary, and a constant gel layer thickness was observed. The two-

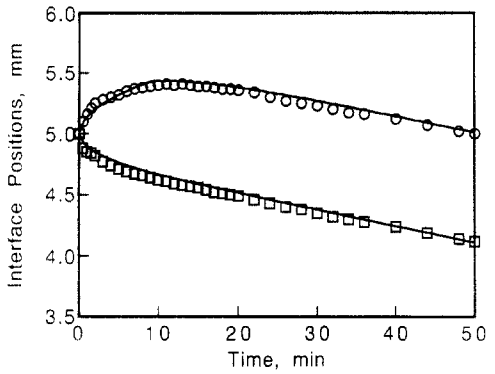

Figure 18. MEK–gel (O) and gel–glassy polystyrene (□) interface positions as a function of time during monodisperse polystyrene dissolution ($\bar{M}_n$ = 620 000) in MEK at 27 °C. The curves represent the prediction of the mathematical model.

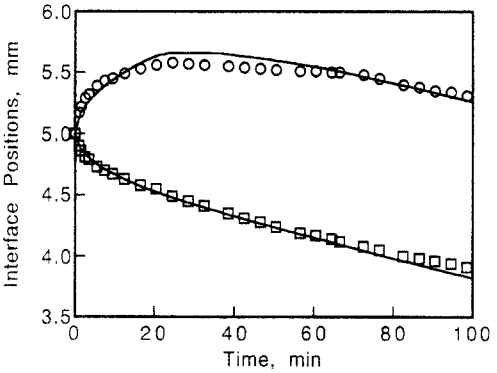

Figure 19. MEK–gel (O) and gel–glassy polystyrene (□) interface positions as a function of time during monodisperse polystyrene dissolution ($\bar{M}_n$ = 1 260 000) in MEK at 27 °C. The curves represent the prediction of the mathematical model.

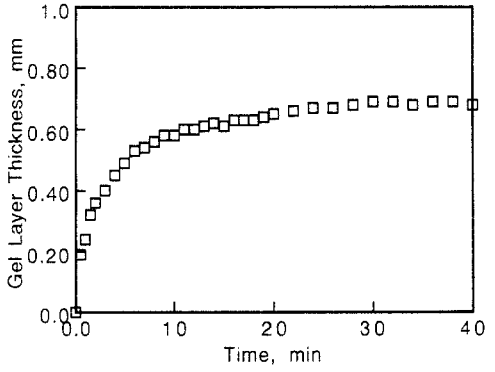

Figure 20. Experimental results of gel layer thickness as a function of time for polystyrene dissolution ($\bar{M}_n$ = 380 000) in MEK at 27 °C.

stage dissolution can be better observed when the gel layer thickness was plotted against time, as for example in Figure 20, which shows the gel layer thickness as a function of time for polystyrene of molecular weight of 380 000.

On the basis of these results, the logarithm of the gel layer thickness was plotted against the logarithm of polystyrene molecular weight as shown in Figure 21, for molecular weights of 28 000–2 830 000. The resultant curve indicated that the dependence of the gel layer thickness on molecular weight is more appreciable in the high molecular weight region.

The above results can be explained by considering two different mechanisms for polymer dissolution: polymer chain disentanglement by reptation and polymer diffusion driven by a concentration gradient. In the high molecular weight region, polymer chains may form a physically cross-linked network and chain entanglement becomes very

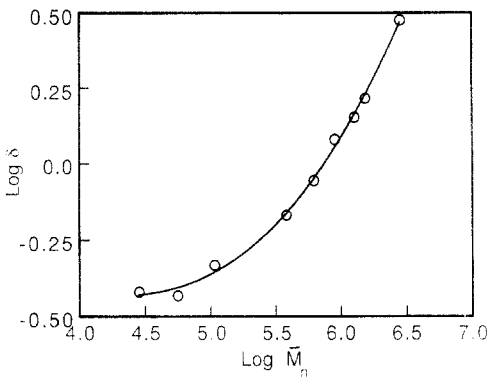

Figure 21. Experimental results of gel layer thickness dependence on polystyrene molecular weight during dissolution in MEK at 27 °C.

significant. As shown in eq 55, the gel layer thickness is dependent on the polymer molecular weight, where the exponent α is 3 if polymer chain disentanglement during the dissolution process is reptation-controlled. Thus, the slope of the logarithm of the gel layer thickness and the logarithm of polymer molecular weight curve is expected to be 1.5. The data of Figure 21 were fitted to a third-order polynomial.

$$\ln \delta = -0.4764 + 0.6102 \ln \bar{M}_n - 0.2753(\ln \bar{M}_n)^2 + 0.03149(\ln \bar{M}_n)^3 \quad (80)$$

The slope of the curve at $\bar{M}_n$ = 2 830 000 was 0.99. If the curve was extrapolated to $\bar{M}_n$ = 10 000 000, the slope was 1.39. This indicates that the chain disentanglement in the very high molecular region can be described as a reptation-controlled process.

As the polymer molecular weight decreases, the effect of the concentration gradient becomes increasingly important. The lowest molecular weight used in our experiments was 28 000, which is lower than the critical molecular weight of polystyrene (M_c = 38 000). Below the critical molecular weight, the polymer concentration gradient becomes the predominant mechanism controlling the dissolution movement of polymer chains from the gel layer to bulk solvent.

Dissolution studies of PMMA were also performed in the present work using the critical angle illumination microscope. The number average molecular weight of the samples tested was $\bar{M}_n$ = 153 000, and the polydispersity index was 2.82. It was observed that PMMA dissolution in MEK did not exhibit initial swelling and that there was no visible gel layer. After a period of time, crazes appeared at the MEK–PMMA interface. The crazes gradually developed into cracks and formed many small fragments (see Figure 22). Thus, PMMA dissolution in MEK is controlled by crack propagation.

Crazing, crack, and the long diffusion induction time are major characteristics of case II transport. The negligible gel layer observed in the dissolution of PMMA can be explained by the relative ratio of the characteristic polymer disentanglement time to the characteristic polymer relaxation time, the modified dissolution number in eq 59. The smaller the dissolution number, the thinner the gel layer. For case II transport, the disentanglement time is much shorter than the polymer relaxation time, and the dissolution number is very small.

Comparison between Modeling and Experimental Results. The results of the previous studies were fitted to the solution of model presented here. Since MEK diffusion in polystyrene is quasi-Fickian, the solution of

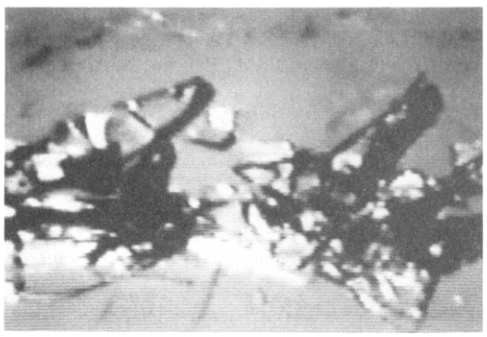

Figure 22. Cracking of a PMMA sample during dissolution in MEK.

eqs 1–4 could be used for the analysis. For this analysis, a number of physical properties and other parameters were used for the system of MEK/polystyrene as described in the section Solution of Mathematical Model. The density of polystyrene was $\rho_2 = 1.05$ g/cm^3, the molar volume of MEK was $\bar{V}_1 = 89.4$ cm^3/mol, the interaction parameter for the MEK/polystyrene system was $\chi = 0.49$, and the critical molecular weight of polystyrene was 38 000. For samples with polymer molecular weight larger than 200 000, the solvent volume fraction was 0.63, as verified by experimental measurements of the solvent concentration in the gel layer. The critical gel volume fraction was $v_{1,g} = 0.18$, as obtained from sorption experiments.

The MEK self-diffusion coefficient at zero MEK concentration was obtained by spin-echo NMR as 1.1×10^{-10} cm^2/s. Vrentas and Duda[51] proposed a relation to relate the mutual diffusion coefficient to the solvent self-diffusion coefficient data. However, one of the major assumptions of this equation was that the solvent concentration is close to zero, and it cannot be applied to polymer dissolution where the solvent volume fraction is generally more than 0.5. In the present work, eq 5 was used. It has been reported[52] that the mutual diffusion coefficient for a MEK/polystyrene system at a MEK volume fraction of 0.5 is about 2×10^{-6} cm^2/s. Using this value and D_0 obtained from our NMR experiments, the coefficient a_d in eq 5 was calculated to be 20. According to the scaling law expression for the dependence of the gel layer thickness on polymer molecular weight, the term α was obtained from Figure 21 by calculating the slope of the log δ vs log $\bar{M}_n$ curve. At $\bar{M}_n$ of 620 000, the slope was 0.6 and α was 1.2. The value of β reflects the dependence of the disentanglement time on polymer concentration. For the MEK/polystyrene system, the polymer volume fraction at the gel–glassy interface was about 0.8 and the polymer volume fraction at the solvent–gel interface was about 0.4. As shown in eq 76, the disentanglement time at the gel–glassy interface is 2^β times longer than that at the solvent–gel interface. If the difference between the two times is 4 orders of magnitude, β is 15. Finally, k_d is independent of molecular weight and can be obtained from the experimental data for one molecular weight sample.

Figures 17–19 present a comparison of the theoretically predicted curves of the front positions as functions of time with the experimental results obtained for the MEK/polystyrene system. It can be seen that the new theoretical model has a remarkable ability to predict the experimental values in a wide range of molecular weights of polystyrene. The only slight deviation was for the sample of molecular weight of 1 260 000, where a possible cause for the deviation is the polydispersity of the sample (PI = 1.13).

Conclusions

A new polymer dissolution model was developed by incorporating the polymer chain disentanglement mechanism into the relevant transport equations. An expression for the disentanglement time was derived from the reptation theory, and the concept of dissolution clock was introduced as a material clock controlling the moving position of the solvent–polymer boundary. The dependences of the gel layer thickness and the polymer dissolution rate on polymer molecular weight were derived, showing that, if the disentanglement time is proportional to M^α, the gel layer thickness is proportional to $M^{\alpha/2}$ and the dissolution rate is proportional to $M^{-\alpha/2}$. A dimensionless dissolution number was defined as the ratio of the characteristic polymer disentanglement time to the characteristic solvent diffusion time and shown to be proportional to the square of the gel layer thickness. Numerical simulation of one-dimensional dissolution showed three distinct dissolution stages and confirmed the proposed scaling law relations for the gel layer thickness and the dissolution rate.

Experimental studies of dissolution of polystyrene and poly(methyl methacrylate) in methyl ethyl ketone were performed. The experimental results showed the dependence of the gel layer thickness on molecular weight is more prominent in the high molecular weight region. The dissolution of PMMA in MEK was controlled by crack propagation, and no significant gel layer was formed.

Acknowledgment. This work was supported in part by Grant CTS-92-12482 from the National Science Foundation. It was presented in part at the Annual AIChE Meeting in November 1993 and the Israeli Institute of Chemical Engineers Meeting in April 1994. We are indebted to P. I. Lee of the University of Toronto, P. Colombo of the University of Parma, and B. Narasimhan of Purdue University for valuable discussions, and to J. M. Caruthers for suggesting the use of a dissolution clock by analogy to viscoelastic problems.

References and Notes

(1) O'Brien, M. J.; Soane, D. S. In *Microelectronics Processing: Chemical Engineering Aspects*; Hess, D. W., Jensen, K. F., Eds.; American Chemical Society: Washington, DC, 1989.
(2) Colombo, P.; Gazzaniga, A.; Caramella, C.; Conte, U.; Manna, A. L. *Acta Pharm. Technol.* **1987**, *33* (1), 15.
(3) Conte, U.; Colombo, P.; Gazzaniga, A.; Sangalli, M. E.; Manna, A. L. *Biomaterials* **1988**, *9*, 489.
(4) Plaizier-Vercammen, J.; van Molle, M. *S.T.P. Pharma Sci.* **1991**, *1*, 267.
(5) Wielgolinski, L. J. *Polym. Prepr. (Am. Chem. Soc., Div. Polym. Chem.)* **1991**, *32* (2), 135.
(6) Ueberreiter, K. In *Diffusion in Polymers*; Crank, J., Park, G. S., Eds.; Academic: New York, 1968.
(7) Ueberreiter, K.; Asmussen, F. *J. Polym. Sci.* **1962**, *57*, 187.
(8) Asmussen, F.; Ueberreiter, K. *J. Polym. Sci.* **1962**, *57*, 199.
(9) Ouano, A. C. *Polym. Eng. Sci.* **1978**, *18*, 306.
(10) Ouano, A. C.; Carothers, J. A. *Polym. Eng. Sci.* **1980**, *20*, 160.
(11) Rodriguez, F.; Krasicky, P. D.; Groele, R. J. *Solid State Technol.* **1985**, *28*, 125.
(12) Cooper, W. J.; Krasicky, P. D.; Rodriguez, F. *Polymer* **1985**, *26*, 1069.
(13) Cooper, W. J.; Krasicky, P. D.; Rodriguez, F. *J. Appl. Polym. Sci.* **1986**, *31*, 65.
(14) Krasicky, P. D.; Groele, R. J.; Jubinsky, J. A.; Rodriguez, F. *Chem. Eng. Commun.* **1987**, *54*, 279.
(15) Groele, R. J.; Rodriguez, F. *J. Coatings Tech.* **1989**, *66*, 55.
(16) Parsonage, E. E.; Peppas, N. A. *Br. Polym. J.* **1987**, *19*, 469.
(17) Parsonage, E. E.; Peppas, N. A.; Lee, P. I. *J. Vac. Sci. Technol.* **1987**, *B5*, 538.
(18) Harland, R. S.; Gazzaniga, A.; Sangani, M. E.; Colombo, P.; Peppas, N. A. *Pharm. Res.* **1988**, *5*, 488.
(19) Drummond, R. K.; Boydston, G. L.; Peppas, N. A. *J. Appl. Polym. Sci.* **1990**, *39*, 2267.
(20) Manjkow, J.; Papanu, J. S.; Hess, D. W.; Soane, D. S.; Bell, A. T. *J. Electrochem. Soc.* **1987**, *134*, 2003.
(21) Manjkow, J.; Papanu, J. S.; Hess, D. W.; Soane, D. S.; Bell, A. T. *J. Appl. Phys.* **1987**, *62*, 682.

(22) Papanu, J. S.; Hess, D. W.; Soane, D. S.; Bell, A. T. *J. Electrochem. Soc.* **1989**, *136*, 3077.
(23) Rao, V.; Frank, C. W.; Pease, R. F. W.; Kosbar, L. O. Abstracts AIChE Meeting, November 1991; Abstract 17f.
(24) Tu, Y.-O.; Ouano, A. C. *IBM J. Res. Dev.* **1977**, *21*, 131.
(25) Lee, P. I.; Peppas, N. A. *J. Controlled Release* **1987**, *6*, 207.
(26) Papanu, J. S.; Soane, D. S.; Bell, A. T. *J. Appl. Polym. Sci.* **1989**, *38*, 859.
(27) Brochard, F.; de Gennes, P. G. *PhysicoChemical Hydrodynamics* **1983**, *4*, 313.
(28) Herman, M. F.; Edwards, S. F. *Macromolecules* **1990**, *23*, 3662.
(29) Alfrey, T., Jr.; Gurnee, E. F.; Lloyd, W. G. *J. Polym. Sci.* **1966**, *C12*, 249.
(30) Hopfenberg, H. B.; Frisch, H. L. *J. Polym. Sci., Polym. Phys. Ed.* **1969**, *7*, 405.
(31) Thomas, N. L.; Windle, A. H. *Polymer* **1982**, *23*, 529.
(32) Durning, C. J. *J. Polym. Sci., Polym. Phys. Ed.* **1985**, *23*, 1831.
(33) Wu, J. C.; Peppas, N. A. *J. Polym. Sci., Polym. Phys. Ed.*, in press.
(34) Flory, P. J. *Principles of Polymer Chemistry*; Cornell University Press: Ithaca, NY, 1953.
(35) Graessley, W. W. *Adv. Polym. Sci.* **1974**, *16*, 1.
(36) Barton, A. F. M. *Handbook of Polymer–Liquid Interaction Parameters and Solubility Parameters*; CRC Press: Boca Raton, FL, 1990.
(37) Hopkins, I. N. *J. Polym. Sci.* **1958**, *28*, 631.
(38) Moreland, L. W.; Lee, E. H. *Trans. Soc. Rheol.* **1960**, *4*, 233.
(39) Lustig, S. R.; Caruthers, J. M.; Peppas, N. A. *Chem. Eng. Sci.* **1992**, *47*, 3037.
(40) de Gennes, P. G. *Scaling Concepts in Polymer Physics*; Cornell University Press: Ithaca, NY, 1979.
(41) de Gennes, P. G.; Leger, L. *Annu. Rev. Phys. Chem.* **1982**, *33*, 49.
(42) de Gennes, P. G. *J. Chem. Phys.* **1971**, *55*, 572.
(43) Edwards, S. F. *Proc. Phys. Soc.* **1967**, *92*, 9.
(44) Leger, L.; Hervet, H.; Rondelez, F. *Macromolecules* **1981**, *14*, 1732.
(45) Wesson, J. A.; Noh, I.; Kitano, T.; Yu, H. *Macromolecules* **1984**, *17*, 782.
(46) Vrentas, J. S.; Jarzebski, C. M.; Duda, J. L. *AIChE J.* **1975**, *21*, 894.
(47) Wu, J. C.; Peppas, N. A. *J. Appl. Polym. Sci.* **1993**, *49*, 1845.
(48) Frisch, H. L. *Polym. Eng. Sci.* **1980**, *20*, 2.
(49) von Meerwall, E. D. *Adv. Polym. Sci.* **1983**, *54*, 1.
(50) Fox, T. G.; Allen, V. R. *J. Chem. Phys.* **1964**, *41*, 344.
(51) Vrentas, J. S.; Duda, J. L. *AIChE J.* **1979**, *25*, 1.
(52) Asmussen, F.; Ueberreiter, K. *Kolloid Z. Z. Polym.* **1968**, *233*, 6.